Contrasting patterns of ERK activation in the tail of the striatum in response to aversive and rewarding signals

Giuseppe Gangarossa[1,2*], Laia Castell[1], Liliana Castro[3], Pauline Tarot[1], Frederic Veyrunes[4], Pierre Vincent[3], Federica Bertaso[1], Emmanuel Valjent[1*]

[1] IGF, CNRS, INSERM, University of Montpellier, Montpellier, France

[2] Université Paris Diderot, Sorbonne Paris Cité, Unité de Biologie Fonctionnelle et Adaptative, CNRS UMR 8251, Paris, France

[3] Sorbonne Université, CNRS, Biological Adaptation and Ageing, F-75005, Paris, France.

[4] Institut des Sciences de l'Evolution de Montpellier, ISEM, Université de Montpellier, CNRS, IRD, EPHE, Montpellier, France

*** correspondence to:** GG (giuseppe.gangarossa@univ-paris-diderot.fr) and EV (emmanuel.valjent@igf.cnrs.fr)

Running title: ERK, dopamine and the caudal striatum

Keywords: striatum, dopamine, ERK, D1R, D2R, psychostimulants

Abstract

The caudal part of the striatum, also named the tail of the striatum (TS), defines a fourth striatal domain. Determining whether rewarding, aversive and salient stimuli regulate the activity of striatal spiny projections neurons (SPNs) of the TS is therefore of a paramount importance to understand its functions, which remain largely elusive. Taking advantage of genetically encoded biosensors (AKAR3) to record PKA signals and by analyzing the distribution of D1R- and D2R/A2aR-SPNs in the TS, we characterized three evolutionary highly conserved subterritories: a D2R/A2aR-lacking area, a D1R/D2-SPNs-enriched and an D1R/D2R-intermingled area. The analysis of ERK phosphorylation in these TS subterritories in response to distinct appetitive, aversive and pharmacological stimuli revealed that SPNs of the TS are not recruited by stimuli triggering innate or learned avoidance responses, fasting, satiety or palatable signals. In contrast, D1R-SPNs of the intermingled and D2R/A2AR-lacking areas are strongly activated by both direct stimulation of D1R and psychostimulant drugs (d-amphetamine, cocaine, MDMA or methylphenidate), but not by hallucinogens. Finally, a similar pattern of ERK activation was observed by blocking selectively dopamine reuptake. Together, our results reveal that the caudal TS might participate in the processing of specific reward signals.

Abbreviations

serotonin (5-HT), adenosine A2a receptor (A2aR), amygdalostriatal transition area (AST), cyclic adenosine monophosphate (cAMP), dopamine D1 receptor (D1R), dopamine D2 receptor (D2R), dopamine (DA), dopamine- and cAMP-regulated phosphoprotein Mr 32 kDa (DARPP-32), dopamine transporter (DAT), enhanced green fluorescence protein (eGFP), extracellular signal-regulated kinase (ERK), 2,5-dimethoxy-4-iodoamphetamine (DOI), dorsal striatum (DS), lateral geniculate nucleus of the thalamus (LGN), medial geniculate nucleus of the thalamus (MGN), 3,4-methyl enedioxymethamphetamine (MDMA), norepinephrine (NE), norepinephrine transporter (NET), phencyclidine (PCP), phosphodiesterase type 4 (PDE4), phosphodiesterase type 10 (PDE10A), protein kinase A (PKA), pentylenetetrazole (PTZ), rostral part of the dorsal striatum (rDS), red fluorescent protein (RFP), Research Resource Identifier (RRID), serotonin transporter (SERT), striatal projection neurons (SPNs), substantia nigra pars compacta (SNc), tail of the striatum (TS), vesicular glutamate type 2 (VGLUT2), ventral posterior nucleus (VPN)

Introduction

The striatum, the main input structure of the basal ganglia circuit, controls distinct functions ranging from motor actions to reward processing and motivated behaviors (Nicola 2007; Gerfen and Surmeier 2011; Graybiel and Grafton 2015; Balleine *et al.* 2007). This functional diversity in part relies on its ability to dynamically integrate multimodal excitatory inputs arising from the cortex and the thalamus (Huerta-Ocampo *et al.* 2014). These excitatory inputs are topographically segregated, delineating functional boundaries between the three classical striatal domains that include sensorimotor, associative and limbic domains (Belin *et al.* 2009; Yin and Knowlton 2006; Gruber and McDonald 2012).

However, recent large-scale mouse projectome studies support the existence of a fourth domain (Hunnicutt *et al.* 2016; Menegas *et al.* 2015). Corresponding to the tail of the striatum (TS), this domain is densely innervated by excitatory inputs from the entorhinal, auditory and visual cortices and sensory thalamic nuclei including the lateral and medial geniculate thalamus and the ventral posterior nucleus (Menegas *et al.* 2015; Jiang and Kim 2018; Gangarossa *et al.* 2013b; Hunnicutt *et al.* 2016). The integration of the information arising from these cortical and thalamic areas is modulated by dopaminergic (DA) neurons clustered in the lateral part of the substantia nigra pars compacta (SNc) (Gangarossa *et al.* 2013b; Menegas *et al.* 2015; Poulin *et al.* 2018). These DA neurons, which express VGLUT2 and lack D2 autoreceptors (Gangarossa *et al.* 2013b; Poulin *et al.* 2018), contribute to reinforcement learning that promotes avoidance of threatening stimuli (Menegas *et al.* 2018).

In addition to its specialized inputs connectivity, the TS is also characterized by a topographic non-random distribution of striatal projection neurons (SPNs) expressing

D1R (D1R-SPNs) and D2R/A2aR (D2R/A2aR-SPNs). Indeed, we have previously identified in the TS a territory lacking D2R/A2aR-SPNs and exclusively composed of D1R-SPNs (Gangarossa *et al.* 2013b). Although this peculiar organization suggests that information processed within the TS could differ from the one described in the sensorimotor, associative and limbic domains, the nature of the stimuli that recruit the SPNs of the TS remain largely unknown.

The present study aims to determine whether stimuli of different nature (rewarding, aversive and salient) modulate the activation of SPNs in the TS. We first performed an accurate characterization of the distribution of D1R- and D2R/A2aR-SPNs within the TS, which allowed us to delineate three striatal subterritories, namely the (*i*) intermingled area, the (*ii*) D2R/A2aR-lacking area and the (*iii*) amygdalostriatal transition (AST) area. We also analyzed the ability of distinct appetitive, aversive and pharmacological stimuli to activate caudal SPNs by monitoring ERK phosphorylation (P-ERK), used here as a molecular readout of striatal activation (Girault *et al.* 2007; Bertran-Gonzalez *et al.* 2010; Hutton *et al.* 2017; Gangarossa *et al.* 2013c). Our results reveal opposing patterns of ERK activation in the TS in response to innate or learned avoidance behaviors compared to rewarding experiences evoked by psychostimulant drugs.

Materials and methods

Animals

C57BL6/J (n = 96) (Charles River, France, RRID:SCR_003792), *Drd2*-eGFP (n = 53) (RRID:MMRRC_000230-UNC), *Nr4a1*-eGFP (n = 7) (RRID:MMRRC_012015-UCD) (Gong *et al.* 2003) and *Drd2*-eGFP/*Drd1a*-tdTomato (n = 4, kindly provided by C Kellendonk, Columbia University, NY USA) mice were used in the present study. Male 8-10 week-old mice were housed in groups of 2 to 5 per cage and maintained in a 12 h light/dark cycle (lights on from 7:30 am to 7:30 pm), in stable conditions of temperature (22°C) and humidity (60%), with food and water provided *ad libitum*. The nine wild mouse taxa from the genus *Mus* which include 3 subspecies of *Mus musculus* [*Mus musculus domesticus* (n = 2), *Mus musculus castaneus* (n = 2) and *Mus musculus musculus* (n = 2)], 4 species of the subgenus *Mus* [*Mus spretus* (n = 2), *Mus spicilegus* (n = 2), *Mus macedonicus* (n = 2) and *Mus caroli* (n = 2)] and 2 species from other *subgenera* (*Nannomys minutoides* (n = 2) and *Coelomys pahari* (n = 2)) were purchased from the Wild Mouse Genetic Repository of Montpellier (France) except *Nannomys minutoides* that are raised at the breeding facility (CECEMA) of the University of Montpellier, France. Male 3-4 month-old Mongolian gerbils (n = 3) (Janvier Laboratories, France) were kindly provided by Gilles Desmadryl (INM Montpellier France). Male Sprague-Dawley rats (n = 3) were purchased from Charles River (France) were also used in the present study. All experiments were performed during the light phase (10 am to 4 pm). For behavioral and pharmacological experiments arbitrary assignments were used to allocate mice to specific groups. No blinding was performed for animal experiments. Housing and experimental procedures were approved by the French Agriculture and Forestry Ministry (C34-172-13). Experiments were performed in accordance with the animal

welfare guidelines 2010/63/EC of the European Communities Council Directive regarding the care and use of animals for experimental procedures.

Drugs and treatment

Drugs and treatment are detailed in Table 1. For *in vivo* pharmacological experiments, mice were habituated to handling and saline injections three consecutive days before the experiment. Drugs were dissolved in 0.9% (w/v) NaCl (saline) and administered on day 4. All the mice were injected in the home cage and perfused 15 or 30 min after injection.

Animal behaviors

Auditory fear conditioning. The experiments were carried out in a fear conditioning apparatus comprising two test boxes placed within ventilated and soundproof cubicles (Imetronic, Pessac, France). Two different contextual configurations were used for the conditioning (box A: smooth white foam on the walls, square cage, metal grid, smooth floor; box B: dark honeycomb foam on the walls, circle cage, metal grid, rough floor). Boxes were cleaned before and after each session with 70% ethanol. After 10 min of habituation to box A or B, mice received 5 pairings of one tone (CS+, 10 s) with an unconditioned stimulus (US: 0.6 mA scrambled footshock, 2 s, coinciding with the last 2 s of CS+ presentation). The interval between each pairing was randomly assigned between 35 and 60 s. The session finished 30 seconds after the end of the last CS+. Freezing behavior was recorded using a tight infrared frame and the threshold for considering freezing behavior was set up at 2 seconds. The first 10 min of habituation were used to assess the basal freezing. Mice were perfused immediately after conditioning.

Active avoidance. The experiments were carried out in a shuttle box placed within a ventilated and soundproof cubicle (Imetronic, Pessac, France). The apparatus consists of two square compartments (20 cm x 20 cm) separated by a partition. Each compartment is equipped with metal grid, independent houselights and tight infrared beams frame to measure locomotor activity. Between each session the apparatus is cleaned with 70% ethanol. Mice are first subjected to a habituation session during which they are exposed to 10 alternating presentations of two different tones (8 s). The two tones are stopped as soon as mice move to the adjacent compartment. A conditioning session (30 min) comprises 30 training trials. A training trial consists of a 8 s avoidance interval, followed by a 5 s escape interval. During the avoidance interval, a tone (CS+) is presented for the duration of the interval or until the mice shuttle (avoid) to the other compartment. If the animal avoided, the CS+ was terminated and no escape interval was presented. If the animal did not avoid, an unconditioned stimulus (US: 0.7 mA scrambled footshock coinciding with the last 5 s of CS+ presentation) was delivered to the mice through the grid floor of the occupied half of the shuttle box. The US motivates the animal to move to the other compartment (escape) terminating the trial. During the intertrial interval, the animal awaits the next trial and is free to cross between compartments at will. During the conditioning session mice are also randomly exposed to the other tone (CS-, 8 s), which is never associated with the US. The percentage of avoidances is used as an index of the learning performance. Mice were perfused immediately after the first or the second conditioning session.

Resident-intruder. This test is based on territory defensive behaviors against unfamiliar intruding conspecifics. A single-housed resident male (FVB/N background mice) was confronted in its home cage by a group-housed intruder male C57/Bl6

mouse for 10 min. Both the resident and intruder were perfused immediately after the test.

Natural stressors. The mice were habituated in a medium-sized box during the first day. Twenty-four hours later the animal was transferred to the same cage adding a petri dish containing its own bedding. After 15 min, a petri dish containing rat bedding is introduced in the cage for 15 min. For the experiment in which the component of for odor 2,3,5-Trimethyl-3-thiazoline (TMT) was used as a predator odor, medium-sized boxes were used without bedding. On the test day, after 15 min of habituation, a petri dish containing a filter paper impregnated with 20 μl of TMT was introduced in the box during 15 min. All mice were perfused immediately after the 15 min exposure of mouse bedding, rat bedding or TMT.

Food-related behavior. Mice were single-housed during the whole protocol. Five groups of mice were used: (1) a control group with *ad libitum* access to chow pellets, (2) a fasted group food deprived for 12 hours (dark period), (3) a group of fasted/refed mice (one cycle), (4) a group of fasted/refed mice during six cycles and (5) a group of bingeing mice daily exposed to high-fat high-sugar (HFHS) diet during 1h/day. All mice were perfused with PFA 4% 30 min following the last exposure to food (chow or HFHS diet).

Tissue preparation and immunofluorescence

Tissues were prepared as previously described (Gangarossa *et al.* 2013a). Thirty µm-thick sections were cut with a vibratome (Leica, France, RRID:SCR_008960) and stored at −20°C in a solution containing 30% (vol/vol) ethylene glycol, 30% (vol/vol) glycerol, and 0.1 M sodium phosphate buffer, until they were processed for immunofluorescence. Striatal sections were identified using the mouse brain atlas (Franklin, K. and Paxinos, G. 2008) and sections comprised between -1.40 to -1.70

mm from bregma were included in the analysis. Sections were processed as follows: free-floating sections were rinsed three times 10 minutes in Tris-buffered saline (TBS, 50 mM Tris–HCL, 150 mM NaCl, pH 7.5). After 15 minutes incubation in 0.2% (vol/vol) Triton X-100 in TBS, sections were rinsed in TBS again and blocked for 1 hour in a solution of 3% BSA in TBS. Sections were then incubated overnight or for 72 hours at 4°C in 1% BSA, 0.15% Triton X-100 with the primary antibodies (Table 2). Sections were rinsed three times for 10 minutes in TBS and incubated for 45 minutes with goat Cy3-coupled (1:400, Jackson Immunoresearch) and goat Alexa Fluor 488 (1:400, Life Technologies) antibodies. Sections were rinsed for 10 minutes twice in TBS and twice in Tris-buffer (1 M, pH 7.5) before mounting in DPX (Sigma-Aldrich). Confocal microscopy and image analysis were carried out at the Montpellier RIO Imaging Facility. All images covering the TS were single confocal sections acquired using sequential laser scanning confocal microscopy (Leica SP8) and stitched together as a single image. Double-labeled images from each region of interest were also single confocal sections obtained using sequential laser scanning confocal microscopy (Leica SP8 and Zeiss LSM780). eGFP-immunopositive cells were pseudocolored cyan and other immunoreactive markers were pseudocolored magenta or yellow as indicated in figures. Images used for quantification were all single confocal sections. Cells were considered positive for a given marker (eGFP and P-ERK) only when the nucleus was clearly visible. Quantification was performed manually using the cell counter plugin of the ImageJ software (RRID:SCR_003070) taking as standard reference a fixed threshold of fluorescence. Figures represent the number of neurons averaged from three adjacent sections.

Brain slices preparation

Experiments were performed with 8-11 days old C57Bl/6J mice obtained from Janvier (Le Genest Saint Isle, France). Mice were housed under standardized conditions with a 12 hrs light/dark cycle, stable temperature (22 ± 1°C), controlled humidity (55 ± 10%) and food and water *ad libitum*. All animal procedures were performed in accordance with the Sorbonne University animal care committee regulations and the French Ministry of Agriculture and Forestry guidelines for handling animals. The protocol has been described previously in more details (Yapo *et al.* 2017). Briefly, 300 µm-thick coronal brain slices of were cut with a VT1200S microtome (Leica, RRID:SCR_008960). Slices were prepared in an ice-cold solution of the following composition: 125 mM NaCl, 0.4 mM CaCl2, 1 mM MgCl2, 1.25 mM NaH2PO4, 26 mM NaHCO3, 20 mM glucose, 2.5 mM KCl, 5 mM sodium pyruvate and 1 mM kynurenic acid, saturated with 5% CO2 and 95% O2. The slices were incubated in this solution for 30 minutes and then placed on a Millicell-CM membrane (Millipore) in culture medium (50% Minimum Essential Medium, 50% Hanks' Balanced Salt Solution, 5.5 g/L glucose, penicillin-streptomycin, Invitrogen). We used the Sindbis virus as a vector to induce expression of the AKAR3 biosensors after overnight incubation. The coding sequences of AKAR3 (Allen and Zhang 2006) were inserted into the viral vector pSinRep5 (Invitrogen, San Diego, CA). This viral vector was added on the brain slices (~5 x 10^5 particles per slice), and the infected slices were incubated overnight at 35°C under an atmosphere containing 5% CO2. Before the experiment, slices were incubated for 30 min in the recording solution (125 mM NaCl, 2 mM CaCl2, 1 mM MgCl2, 1.25 mM NaH2PO4, 26 mM NaHCO3, 20 mM glucose, 2.5 mM KCl and 5 mM sodium pyruvate saturated with 5% CO2 and 95% O2). Recordings were performed with a continuous perfusion of the same solution at 32°C.

Biosensor imaging and data analysis

Live imaging was performed on brain slices, which expressed the AKAR3 biosensor (Polito *et al.* 2014). Slices were kept at room temperature in the recording solution saturated with 5% CO2 and 95% O2 for around 30 minutes before imaging. The composition of the recording solution was the same as the slicing solution except that it contained no kynurenic acid and CaCl2 was 2 mM. The slice was imaged in a temperature controlled (32°C) recording chamber and continuously perfused at 2 ml/min using a peristaltic pump. The same perfusion system was used to apply drugs (SKF38393, Cat. #0922; CGS21680, Cat. #1063; Forskolin, Cat. #1099 purchased from Tocris, RRID:SCR_003689) onto the recorded slice. Wide field imaging was performed using Olympus BX50WI or BX51WI upright microscopes with a 40X 0.8 NA water immersion objective. The donor excitation was provided by an LED source (420 nm diode, Mightex) with a HC434/17 excitation filter (Semrock). The dichroic mirror was BS452 (Semrock). Two images were acquired for every data point by alternating filter for donor (HC479/40) and acceptor (HC542/50 both from Semrock) emission with a filter wheel (Sutter Instruments). Images were acquired using an ORCA-AG camera (Hamamatsu). Image acquisition was controlled using iVision software (Biovision, RRID:SCR_005057).

Data analysis was done with custom routines written in IGOR Pro (Wavemetric, RRID:SCR_000325) following the previously described protocol (Polito *et al.* 2014; Yapo *et al.* 2017). FRET changes were quantified using ratio of images from donor and acceptor channels for each data point. Corrections for non-uniform illumination, movement and channel mis-registration were done prior to ratio calculation. No corrections for bleed-through or cross-excitation were applied. The ratio value for a region-of-interest (ROI) was calculated by averaging all the individual pixels included

in that ROI, weighted by their intensity. Unresponsive cells to either D1R or A2aR agonists were excluded.

Statistical analysis

All statistical comparisons were performed with two-sided tests in Prism 6 (GraphPad Software, La Jolla, CA, USA, RRID:SCR_002798). The distribution of data was determined with Shapiro-Wilk normality test. No sample size calculations were performed. To determine outliers in every experimental group we performed the Grubbs' test in Prism (RRID:SCR_002798). No outliers were identified. All the data were analyzed using one-way ANOVA, where treatment was the independent variable, followed by Bonferroni *post hoc* test for specific comparisons. Student *t-test* with equal variances was used when relevant. In all cases, significance threshold was set at $p < 0.05$.

Results

Distribution of D1R- and D2R-SPNs in the TS is unique

Drd2-eGFP/*Drd1a*-tdTomato transgenic mice were used to characterize the distribution of D1R- and D2R-expressing SPNs in the TS. The analysis of eGFP (D2R-SPNs) and RFP (D1R-SPNs) expression revealed that, unlike a large portion of the dorsal striatum (Gangarossa *et al.* 2013b), the distribution of D1R- and D2R-positive cells in the TS is not random. At least three distinct territories can be identified: 1) a large strip adjacent to the GPe that is devoid of D2R/A2aR-SPNs called hereafter the D2R/A2AR-lacking area, 2) an intermingled area in which a random distribution of D1R- and D2R-SPNs is observed, and 3) the amygdalostriatal transition area (AST) characterized by a high percentage of SPNs expressing both D1R and D2R (~33%) (Fig. 1a, b). To confirm this non-random distribution, TS sections of *Drd2*-eGFP mice were used to analyze the endogenous eGFP fluorescence in combination with specific markers of D2R- and D1R-SPNs. D2R and A2aR antibodies, that stain D2R-SPNs dendrites, confirmed the existence of the D2R/A2AR-lacking area. Conversely, the strong D1R labeling confirmed that this subterritory of the TS is composed exclusively of D1R-SPNs (Fig. 1c).

The peculiar distribution of D1R- and D2R/A2aR-SPNs in the TS led us to investigate the responsiveness of SPNs located in the D2R/A2aR-lacking area and the AST in response to the stimulation of D1R and A2aR. In rostral part of the dorsal striatum, stimulation of both receptors yields an increase in cAMP levels and consequent activation of PKA in D1R- and D2R/A2aR-SPNs, respectively (Beaulieu and Gainetdinov 2011; Yapo *et al.* 2017). To address this issue, we performed *ex vivo* real-time PKA imaging in mouse TS slices by using the genetically encoded biosensor, AKAR3 (Yapo *et al.* 2017). In the D2R/A2aR-lacking area, stimulation of

D1R with a saturating dose of SKF38393 (1 μM) yielded a large, but sub-maximal, increase in PKA signals in AKAR3-expressing neurons (Fig. 2a). In contrast, the application of the A2aR agonist, CGS21680 (1 μM), failed to further increase PKA signals. At the end of the experiment, addition of Forskolin (Fsk, 12.5 μM), an activator of adenylyl cyclase, maximally increased the F535/F480 emission ratio (Fig. 2a) (Castro *et al.* 2013). On average, CGS21680 had no effect on the amplitude of the PKA response induced by SKF38393 in the D2R/A2AR-lacking area (67 ± 3% vs 65 ± 2%, of the maximal Fsk response, respectively) (Fig. 2b). On the other hand, in the AST area, the amplitude of PKA responses produced by SKF38393 (62 ± 3% of the maximal Fsk response) was further increased in response to A2aR activation (94 ± 1%) (Fig. 2c, d). These results show that the D2R/A2AR-lacking area expresses functional D1 receptors and lacks A2A receptors, whereas both receptors are functional in the AST region. Together, these results confirm that SPNs of the D2R/A2AR-lacking area only respond to D1 agonist, whereas the AST responds to both D1 and A2aR activation.

Distribution of D1R- and D2R-SPNs in the TS is evolutionary conserved

We next wondered whether a similar organization of the TS might be observed in distinct species of the Muridae family. To explore this issue, we examined the presence of the D2R/A2AR-lacking area indifferent wild mouse species from the genus *Mus*. This genus comprises several species subdivided into four subgenera encompassing about 7 million years of divergence (Chevret and Dobigny 2005; Veyrunes *et al.* 2006) (Fig. 3a). The lack of A2aR immunoreactivity and the strong expression of DARPP-32, a highly conserved marker of all SPNs, are used here to define a molecular fingerprint of the D2R/A2AR-lacking area (Gangarossa *et al.*

2013b). Using this combination of antibodies, we observed that the D2R/A2AR-lacking area is present in all the species examined which include 3 subspecies of the *Mus musculus*, 4 species of *Subgenus Mus* and 2 species of two of the three other *Subgenera* (Fig. 3a-c). A similar organization of the caudal TS was also identified in *Meriones unguiculatus* (Mongolian gerbil) (Fig. 3d) and *Rattus norvegicus* (Fig. 3e). Taken together, our data reveal that the distribution of D1R- and D2R-SPNs in the TS is evolutionary conserved.

Regulation of ERK activation in the TS by aversive signals

Avoidance behaviors have been associated with the activation of the TS (Menegas *et al.* 2018). To determine the impact of aversive stimuli on the TS, we monitored ERK activation by quantifying the number of phosphorylated-ERK (P-ERK) immunoreactive SPNs in the three territories of the TS: the intermingled area, the D2R/A2AR-lacking area and the AST (Table 3).

We first analyzed the level of P-ERK in mice that underwent the resident-intruder assay. The resident and intruder mice were perfused ten minutes after the unfamiliar mouse was placed inside the resident's cage. No significant differences were found in the number of P-ERK-positive neurons in the TS (Table 3). We then tested whether exposure to predator odors was able to modulate P-ERK in the TS. Although mice exposed to rat bedding or 2,3,5-Trimethyl-3-thiazoline (TMT), a component of fox odor, showed strong defensive reactions, ERK activation remained unchanged in all territories of the TS when compared to mice exposed to mouse bedding (Table 3). Taken together, these data suggest that the TS is not recruited by aversive stimuli triggering innate avoidance.

We therefore assessed whether mice exposed to mild footshocks, either unpredictable (US) or signaled by a salient auditory stimulus (arousing but non-nociceptive) (CS-US pairing), displayed an altered P-ERK level in the caudal TS (Table 3). While no changes were observed in the intermingled and D2R/A2AR-lacking areas, a significant reduction in the number of P-ERK-positive SPNs was found in the AST of mice undergoing five CS-US pairings compared to those only exposed to the CS or the US (Table 3). Similarly, mice that learned to avoid mild footshocks during an interval signaled by the presentation of a CS (salient auditory stimulus) displayed a reduced total number of P-ERK-immunoreactive neurons in the TS, though no statistical differences were revealed when the three territories were analyzed separately (Table 3). We finally thought to determine whether prolonged aversive states might alter the levels of P-ERK in the TS. The administration of lithium chloride (LiCl) (150 mg/kg), a compound known to cause nausea and visceral malaise (Yamamoto and Ueji 2011), blunted ERK activation in all TS subterritories (Table 3).

Because the effects induced by the administration of LiCl can also be perceived as potent anorexigenic signals, we investigated whether SPNs of the TS were activated during food deprivation (fasting) and satiation (refeeding). No major differences were observed in the number of P-ERK immunoreactive neurons between mice having *ad libitum* access to chow pellets and mice being fasted for 12 hours followed or not by 1 or 6 cycles of re-feeding schedule (Table 4). Similarly, ERK activation was unchanged in the TS of mice exposed to high-fat high-sugar (HFHS) diet during 1h/day (Table 4). Together, these data suggest that SPNs of the TS are not activated by signals associated with fasting, satiety or palatability.

Psychostimulant drugs promote ERK activation in the TS

Acute d-amphetamine administration activates ERK in striatal and accumbal D1R-SPNs (Valjent *et al.* 2005; Gerfen *et al.* 2008; Gangarossa *et al.* 2013a). We therefore analyzed whether the same treatment was also able to promote ERK phosphorylation in the TS. Immunofluorescence analysis revealed that a single injection of d-amphetamine (10 mg/kg) increases the number of P-ERK-positive neurons in the intermingled and D2R/A2AR-lacking areas of the TS. Of note only a mild increase was observed in the AST (Fig. 4a, b). To clarify in which striatal cell-type ERK activation occurred, *Drd2*-eGFP mice were treated with d-amphetamine and the distribution of P-ERK-positive neurons in D2R-positive and D2R-negative SPNs was analyzed. In line with the observations made in the rostral part of the dorsal striatum (DS) (Valjent *et al.* 2005; Gerfen *et al.* 2008), d-amphetamine-induced ERK phosphorylation in the TS was confined in D2R-negative SPNs, which most likely correspond to D1R-SPNs (Fig. 4c, d). This increase in ERK phosphorylation was rapid and transient since it declined 30 min after the administration of d-amphetamine (Fig. 4d). In the rostral DS, ERK activation induced by d-amphetamine is preferentially concentrated in patches (Biever *et al.* 2015). We therefore thought to determine whether P-ERK-immunoreactive neurons of the caudal TS were also distributed within patches. To do so, we used *Nr4a1*-eGFP mice, a mouse line allowing the delineation of the patch/matrix compartmentalization (Davis and Puhl 2011). The analysis of eGFP expression revealed that eGFP-positive cells were mainly located in the intermingled area whereas only few scattered neurons were detected in the D2R/A2AR-lacking area and AST (Fig. 4e). When d-amphetamine was administrated to *Nr4a1*-eGFP mice, we observed that the increased P-ERK-positive cells occurred preferentially in eGFP-poor zones and was restricted to

Nr4a1-eGFP-negative neurons suggesting that in the TS, ERK activation is not enriched in patch compartments (Fig. 4f).

Finally, we tested whether other psychostimulant drugs shared the same pattern of ERK activation in the TS. As shown in Figure 5, a single injection of methylphenidate (15 mg/kg), MDMA (10 mg/kg) or cocaine (15 mg/kg) increased ERK phosphorylation in the D2R/A2AR-lacking and the intermingled areas in which it was restricted to D2R-negative SPNs. Together, these data revealed that in the TS, D1R-SPNs of the intermingled and D2R/A2AR-lacking areas are activated by psychostimulant drugs.

In addition to its stimulant properties, MDMA is also known to distort sensory and time perception, two features shared by hallucinogenic drugs (Starr *et al.* 2008; Litjens *et al.* 2014). We therefore tested whether other hallucinogen drugs were able to activate SPNs of the TS. The administration of the psychedelic compound, DOI (10 mg/kg), a substituted amphetamine without stimulant effects, failed to induce ERK activation in the TS (Table 5). On the other hand, PCP (3 mg/kg), a NMDA receptor blocker causing hallucinations, reduced P-ERK in the caudal TS (Table 5). This decrease was even more pronounced after the administration of dizocilpine (0.3 mg/kg), another NMDA blocker that also acts as a potent anti-convulsant (Table 5). Because convulsant drugs also trigger ERK activation (Gangarossa *et al.* 2011; Berkeley *et al.* 2002), we examined whether such pharmacological agents were able to regulate ERK phosphorylation in the TS. Indeed, acute administration of PTZ (60 mg/kg) or kainate (20 mg/kg) increased the number of P-ERK-positive neurons exclusively in the AST area (Table 5). Together, these results indicate that, at the level of the TS, distinct classes of pharmacological agents differentially recruit D1R- and D2R/A2aR-SPNs in distinct subsets of striatal territories.

Increased ERK activation in the TS by selective DA reuptake inhibition

Psychostimulant drugs such as d-amphetamine, methylphenidate, cocaine and MDMA mediate their effects in part by acting on monoamines transporters (DAT, NET and SERT). We therefore examined whether the blockade of dopamine, noradrenaline or serotonin reuptake promoted ERK activation in the TS. Administration of GBR12783 (10 mg/kg), a DAT blocker, enhanced ERK phosphorylation preferentially in SPNs of the D2R/A2AR-lacking area and to a lesser extent in the intermingled area (Fig. 6a, b). In contrast, the antidepressant drugs desipramine (20 mg/kg) and fluoxetine (10 mg/kg) which inhibit the reuptake of NE and 5-HT respectively, failed to activate ERK (Fig. 6a, b). Together, these results show that blockade of DA reuptake is sufficient to trigger ERK activation in the TS.

D1R activation is necessary and sufficient to activate ERK in the TS

In the rostral DS and the nucleus accumbens, ERK activation induced by d-amphetamine requires D1R stimulation (Valjent *et al.* 2005). Similarly, blockade of D1R by SCH23390 prevented d-amphetamine-induced ERK phosphorylation in the TS (Fig. 7a, b). However, contrasting results have been obtained regarding the ability of direct stimulation of D1R to promote ERK phosphorylation in the rostral DS (Gerfen *et al.* 2002; Gangarossa *et al.* 2013d). To test the impact of D1R activation, mice were administrated either with SKF81297 (5 mg/kg) or SKF83822 (5 mg/kg), two agonists known to trigger D1R signaling through cAMP production (Kuroiwa *et al.* 2008). Both compounds produced a strong activation of ERK that resembles the one induced by d-amphetamine (Fig. 7c and 4a). In contrast, when we injected SKF83959 (5 mg/kg), a partial agonist at both D1R-mediated adenylate cyclase and β-arrestin recruitment (Lee *et al.* 2014; Jin *et al.* 2003), ERK phosphorylation was

less pronounced (Fig. 7c). A similar regulation was observed after the injection of the non-selective D1R/D2R agonist, apomorphine (3 mg/kg) (Fig. 7c). Together, these results indicate that D1R stimulation is sufficient to activate ERK in the TS.

To determine whether cAMP production was necessary and sufficient to activate ERK in the TS, we artificially increased the cAMP levels by administering papaverine, a potent inhibitor of the striatal-enriched phosphodiesterase isoform PDE10A (Nishi *et al.* 2008). Papaverine (30 mg/kg) induced a robust ERK activation in the TS (Fig. 7d). However, this activation was restricted to the ventral part of the intermingled area and confined in D2R-SPNs (Fig. 7d-f). Because D1R- and D2R-SPNs also expressed PDE4, we also examined the impact of PDE4 inhibition. Administration of rolipram (10 mg/kg) significantly increased ERK phosphorylation in the intermingled area whereas no effects were observed in both the D2R/A2aR-lacking area and the AST (Fig. 7g, h). In this case, increased ERK phosphorylation was detected in both D2R-positive and D2R-negative SPNs (Fig. 7g, h). Together, these results show that D1R stimulation or PDEs inhibition trigger distinct patterns of ERK phosphorylation in the TS.

Discussion

Despite the renewed interest in the caudal part of the striatum (also referred to the tail of the striatum, TS), its anatomo-functional organization remains poorly characterized. In this study, we provide evidence that D1R- and D2R-SPNs of the TS display a unique regional distribution which anatomical features are to some extent evolutionary conserved. In addition, our functional results reveal contrasting patterns of ERK activation in response to aversive and reward signals and suggest that activation of the TS is a common feature of psychostimulant drugs.

The use of BAC transgenic mice has been instrumental in improving our undersatnding of the anatomo-functional organization of striatum (Bertran-Gonzalez *et al.* 2008; Matamales *et al.* 2009). Recent in-depth analyses of the anatomical arrangement of D2R/A2aR- and D1R-SPNs have revealed that the randomness of the distribution of these two neuronal populations varied along the rostro-caudal axis (Gangarossa *et al.* 2013b; Gagnon *et al.* 2017; Ren *et al.* 2017). In fact, while D2R/A2aR- and D1R-SPNs are randomly distributed in the majority of the dorsal striatum (Gangarossa *et al.* 2013b; Ren *et al.* 2017; Wei *et al.* 2018), a segregated anatomical organization has been unveiled in the TS (Gangarossa *et al.* 2013b). We analyzed the distribution of eGFP and RFP-positive cells in the TS in combination with specific markers of D2R- and D1R-SPNs, and extending our previous observations (Gangarossa *et al.* 2013b), we confirmed the existence of a TS D2R/A2aR-lacking area composed exclusively of D1R-expressing SPNs. In addition, the use of *Drd2*-eGFP/*Drd1a*-tdTomato mice allowed us to delineate two additional TS subterritories. The first one, juxtaposed to the D2R/A2aR-lacking area, corresponds to a large territory in which D1R- and D2R-SPNs are evenly intermingled. The direct visualization of D1R- and D2R-SPNs revealed that in the

intermingled area, SPNs co-expressing both D1R and D2R are preferentially clustered adjacently to the corpus callosum. This contrasts with the homogenous distribution previously described in the anterior dorsal striatum (Gagnon *et al.* 2017; Ren *et al.* 2017; Wei *et al.* 2018). The second subterritory, embedded between the striatum and the central amygdala is characterized by a high percentage of D1R/D2R-SPNs (~33%). This area, which most likely corresponds to the amygdalostriatal transition (AST) (Fudge and Haber 2002; Jolkkonen *et al.* 2001), is the striatal subterritory comprising the highest density of D1R/D2R-SPNs, together with the bundle-shaped area of the caudomedial shell of the nucleus accumbens (Gangarossa *et al.* 2013a; Gagnon *et al.* 2017). Although the connectivity and function of this striatal population remain to be established, recent data indicate that D1R/D2R-SPNs display unique morphological features (Gagnon *et al.* 2017) and molecular profile (Gokce *et al.* 2016; Saunders *et al.* 2018). Future studies will be required to determine whether TS D1R/D2R-SPNs share similar features or define another SPNs population.

Our comparative analysis demonstrates that D2R/A2aR- and D1R-SPNs distribution is anatomically conserved across the *Muridae* family (*Rodentia* order). Indeed, even though size and shape slightly differ, the D2R/A2aR-lacking area was unambiguously identified in different wild mouse strains, gerbils and rats. Interestingly, recent high-throughput projectome studies revealed that anatomical origins of cortico- and thalamostriatal sensory inputs innervating the TS are also conversed in rodents (Hintiryan *et al.* 2016; Hunnicutt *et al.* 2016; Jiang and Kim 2018). In both mice and rats, TS SPNs receive convergent excitatory inputs arising from the visual and auditory cortices and TS-projecting DA neurons from the lateral part the SNc (Menegas *et al.* 2015; Hintiryan *et al.* 2016; Hunnicutt *et al.* 2016; Jiang

and Kim 2018; Poulin *et al.* 2018; Deniau *et al.* 1996). Despite anatomical constancy across species, the functional role of the TS has been poorly addressed. Recently two studies revealed that the TS is not essential to promote movement. Indeed, lesion of TS-projecting DA did not affect the time spent moving and the velocity (Menegas *et al.* 2018) and direct activation of TS D1R-SPNs using optogenetic failed to elicit movement (Guo *et al.* 2018). Instead, D1R-SPNs of the TS appear to play an important role in auditory decisions (Guo *et al.* 2018; Xiong *et al.* 2015) and contribute to reinforcement learning that promotes avoidance of threatening stimuli (Menegas *et al.* 2018). Future studies will establish whether causality between aforementioned functions and the activation of D1R-SPNs within specific TS subterritories exist.

Our functional study, assessed by monitoring ERK phosphorylation (i.e. activation), provides important clues concerning the recruitment of SPNs within the TS. While salient and aversive signals are known to activate TS-projecting DA neurons (Menegas *et al.* 2017; Menegas *et al.* 2018), aversive stimuli triggering innate or learned avoidance responses failed to trigger ERK activation in the TS. Instead, our results suggest that TS SPNs activity might depend on the nature of the aversive stimuli. Indeed, we have found that the administration of LiCl, an aversive drug that causes nausea and visceral malaise, blunts ERK activation in TS. This decreased phosphorylation is particularly evident in the AST and the ventral edge of the intermingled area, which both integrate visceral information (Hintiryan *et al.* 2016). Moreover, ERK phosphorylation remains unchanged following fasting, satiety or palatability suggesting that the TS does not appear neither to be sensitive to inner state information associated with feeding behavior. Our survey using various pharmacological agents revealed that TS SPNs are particularly responsive to

psychostimulants drugs. Thus, the administration of d-amphetamine, MDMA, cocaine or methylphenidate increases ERK activation selectively in D1R-SPNs of the D2R/A2aR-lacking area and to a lesser extent in the ventral edge of the intermingled area. Although these drugs share a similar pattern of ERK phosphorylation, a more pronounced activation was observed with d-amphetamine and MDMA compared to cocaine and methylphenidate. The lack of effects of NET and SERT inhibitors combined with the fact that the blockade of DA reuptake triggers a pattern of ERK activation comparable to cocaine or methylphenidate strongly suggest that the mechanisms by which these compounds induce DA release account for the difference observed between amphetamine and cocaine. Because the TS integrates visual and auditory information, future studies will be required to determine whether activation of TS D1R-SPNs contribute to psychostimulant-induced arousal and alertness.

The activation of ERK in the D1R-SPNs of the TS by d-amphetamine is prevented by SCH23390 indicating that, similarly to the rostral part of the dorsal striatum and the nucleus accumbens, D1R activation is required (Valjent *et al.* 2005; Bertran-Gonzalez *et al.* 2008; Gerfen *et al.* 2008). Interestingly, the direct pharmacological stimulation of D1R, using agonists known to trigger D1R signaling through cAMP production (Liu and Graybiel 1998; Kuroiwa *et al.* 2008), is sufficient to activate ERK in the TS. Given the similarity observed between the patterns of ERK phosphorylation induced by D1R agonists and d-amphetamine, it is tempting to hypothesize that common intracellular mechanisms could account for this activation. Thus, the inhibition of ERK dephosphorylation through the cAMP/PKA/DARPP-32 has been shown to be essential to sustain D1R-mediated ERK phosphorylation in the striatum (Valjent *et al.* 2005; Gerfen *et al.* 2008). The triggering events in D1R-

dependent ERK activation, meanwhile, involve synergistic intracellular events. Thus, cAMP-dependent mechanisms involving the PKA-dependent recruitment of Rasgrp2 and/or the activation of the cAMP sensor NCS-Rapgef2 have been recently unveiled (Nagai *et al.* 2016; Jiang *et al.* 2017). Moreover, ERK activation in D1R-SPNs has also been shown to rely on D1Rthe activation of Fyn which, by phosphorylating GluN2B of NMDAR, leads to an increase of calcium influx and a subsequent activation of the Ras-GRF1/ERK cascade (Fasano *et al.* 2009; Pascoli *et al.* 2011; Jin *et al.* 2019). Such cellular events provide a mechanism through which glutamate contribute to the regulation of ERK activation induced by d-amphetamine and D1R agonists (Choe *et al.* 2002; Valjent *et al.* 2005; Pascoli *et al.* 2011). Because TS-projecting DA neurons express VGLUT2 (Root *et al.* 2016; Poulin *et al.* 2014; Poulin *et al.* 2018), future studies will be necessary to determine whether glutamate co-release from these DA neurons is essential for D1R-dependent stimulation of ERK in the TS.

Interestingly, when intracellular cAMP was increased independently of receptors through PDE10A inhibition, the D2R/A2AR-lacking area did not show ERK phosphorylation. This is consistent with previous studies, which showed that PDE10A inhibition increased PKA-dependent phosphorylation levels in D2R-SPNs but not in D1R-SPNs (Polito *et al.* 2015). This difference was demonstrated to result from a powerful action of phosphatase-1 (PP-1), which prevents PKA substrates from remaining phosphorylated, whereas DARPP-32 efficiently inhibits PP1 in D2R-SPNs (Nishi *et al.* 2008; Polito *et al.* 2015). The DARPP-32/PP-1 loop also regulates ERK phosphorylation (Valjent *et al.* 2005), and we therefore hypothesize that the increased ERK phosphorylation in D2R-SPNs in response to PDE10A inhibition results from the same mechanism.

In conclusion, our study provides anatomical and molecular evidence suggesting that the TS can indeed be considered as a fourth striatal domain. Our functional analysis also indicates that the TS is a major target of psychostimulant drugs. Future investigations are now required to decipher the functional implication of TS in the action of these drugs.

Table 1. List of drugs

Drugs	Doses	Catalog N	Supplier (RRID)
d-amphetamine	10 mg/kg, i.p.	Cat. #2813	Tocris RRID:SCR_003689
Cocaine	15 mg/kg, i.p.	Cat. #C5776	Sigma-Aldrich RRID:SCR_008988
MDMA	10 mg/kg, i.p.	Cat. #M5029	Sigma-Aldrich RRID:SCR_008988
Methylphenidate	15 mg/kg, i.p.	Cat. #M2892	Sigma-Aldrich RRID:SCR_008988
GBR12783	10 mg/kg, i.p.	Cat. #0513	Tocris RRID:SCR_003689
Desipramine	20 mg/kg, i.p.	Cat. #3067	Tocris RRID:SCR_003689
Fluoxetine	10 mg/kg, i.p.	Cat. #0927	Tocris RRID:SCR_003689
SKF81297	5 mg/kg, i.p.	Cat. #1447	Tocris RRID:SCR_003689
SKF83822	5 mg/kg, i.p.	Cat. #2075	Tocris RRID:SCR_003689
SKF83959	5 mg/kg, i.p.	Cat. #2074	Tocris RRID:SCR_003689
Apomorphine	3 mg/kg, s.c.	Cat. #2073	Tocris RRID:SCR_003689
SCH23390	0.1 mg/kg, i.p.	Cat. #0925	Tocris RRID:SCR_003689
LiCl	150 mg/kg, i.p.	Cat. #L4408	Sigma-Aldrich RRID:SCR_008988
DOI	10 mg/kg, i.p.	Cat. #D101	Sigma-Aldrich RRID:SCR_008988
Phencyclidine	3 mg/kg, s.c.	Cat. #P3029	Sigma-Aldrich RRID:SCR_008988
Dizocilpine	0.3 mg/kg, i.p.	Cat. #0924	Tocris RRID:SCR_003689
PTZ	60 mg/kg, i.p.	Cat. #P6500	Sigma-Aldrich RRID:SCR_008988
Kainate	20 mg/kg, i.p.	Cat. #K0250	Sigma-Aldrich RRID:SCR_008988
Papaverine	30 mg/kg, i.p.	Cat. #P3510	Sigma-Aldrich RRID:SCR_008988
Rolipram	10 mg/kg, i.p.	Cat. #0905	Tocris RRID:SCR_003689
SKF38393	1 μM	Cat. #0922	Tocris RRID:SCR_003689
CGS21680	1 μM	Cat. #1063	Tocris RRID:SCR_003689
Forskolin	12.5 μM	Cat. #1099	Tocris RRID:SCR_003689

d-amph, d-amphetamine; MDMA, 3,4-Methylenedioxymethamphetamine; LiCl, Lithium chloride; DOI, 2,5-Dimethoxy-4-iodoamphetamine; Dizopilcine, MK801; PTZ, Pentylenetetrazol

Table 2. List of primary antibodies

Antigen	Host	Dilution	Supplier	Catalog N°
eGFP	Chicken	1:1000	Life Technologies	A10262
RFP	Rabbit	1:1000	MBL	PM005
DARPP-32	Rabbit	1:1000	Cell Signaling	#2306
D2R	Guinea Pig	1:1000	Frontier Institute	D2R-GP-Af500
A2aR	Guinea Pig	1:1000	Frontier Institute	A2A-GP-Af1000
D1R	Guinea Pig	1:1000	Frontier Institute	D1R-GP-Af500
P-ERK1/2	Rabbit	1:500	Cell Signaling	#9101

eGFP, enhanced green fluorescent protein; RFP, red fluorescent protein; DARPP-32, Dopamine- and cAMP-regulated phosphoprotein, Mr 32 kDa; D2R, dopamine D2 receptor; A2aR, adenosine A2a receptor; D1R, dopamine D1 receptor

Table 3. Regulation of ERK phosphorylation in the TS by aversive signals

Models/Drugs	Number of P-ERK positive cells			
	Total	**Intermingled**	**D2R/A2aR-lacking**	**AST**
3.1 Resident/Intruder				
Resident (n = 3)	50 ± 5	32 ± 3	9 ± 1	8 ± 1
Intruder (n = 3)	56 ± 3	28 ± 3	14 ± 2	14 ± 2
3.2 Natural stressors				
Mouse bedding (n = 3)	71 ± 6	38 ± 6	10 ± 3	15 ± 1
Rat bedding (n = 3)	66 ± 14	43 ± 10	13 ± 3	10 ± 2
Fox urine (TMT) (n = 3)	52 ± 3	28 ± 3	7 ± 1	17 ± 4
3.3 Cued fear conditioning				
CS (n = 4)	46 ± 15	23 ± 13	3 ± 1	21 ± 2
US (n = 4)	58 ± 5	38 ± 4	3 ± 1	17 ± 2
CS-US (n = 4)	42 ± 4	25 ± 4	4 ± 1	13 ± 1
3.4 Active avoidance				
Day 1 (n = 4)	47 ± 15	28 ± 13	4 ± 1	14 ± 3
Day 2 (n = 5)	14 ± 4*	4 ± 1	2 ± 1	8 ± 2
3.5 Aversive drug				
Saline (n = 4)	53 ± 7	34 ± 7	10 ± 2	9 ± 1
LiCl (n = 3)	8 ± 4**	3 ± 2*	1 ± 1*	4 ± 1*

For detailed statistics see Suppl. Table 5.

CS, conditioned stimulus; US, unconditioned stimulus; TMT, 2,3,5-trimethyl-3-thiazoline; LiCl, Lithium chloride

Table 4. Regulation of ERK phosphorylation in the TS by satiety and palatable signals

Models	Number of P-ERK positive cells			
	Total	**Intermingled**	**D2R/A2aR-lacking**	**AST**
4.1 Food intake				
Control (n = 4)	39 ± 5	29 ± 4	2 ± 1	8 ± 1
Fast (n = 3)	23 ± 6	15 ± 5	2 ± 1	6 ± 1
Fast/re-fed 1 cycle (n = 4)	32 ± 2	21 ± 1	2 ± 1	9 ± 1
Fast/re-fed 6 cycles (n = 4)	49 ± 9	32 ± 7	4 ± 1	13 ± 3
HFHS (n = 4)	36 ± 1	22 ± 2	4 ± 1	10 ± 1

For detailed statistics see Suppl. Table 6.

HFHS, high-fat high-sugar diet

Table 5. Regulation of ERK phosphorylation in the TS by hallucinogens and convulsants

Drugs	Number of P-ERK positive cells			
	Total	**Intermingled**	**D2R/A2aR-lacking**	**AST**
5.1 Hallucinogens				
Control (n = 4)	47 ± 5	29 ± 5	11 ± 1	7 ± 1
DOI (n = 4)	47 ± 8	32 ± 5	5 ± 1	10 ± 3
PCP (n = 3)	25 ± 6	11 ± 1	10 ± 4	4 ± 1
Dizocilpine (n = 3)	4 ± 1***	0 ± 0**	1 ± 1**	3 ± 1
5.2 Convulsants				
Control (n = 3)	33 ± 5	21 ± 2	4 ± 2	8 ± 1
PTZ (n = 3)	72 ± 7	27 ± 2	7 ± 1	38 ± 7**
Kainate (n = 3)	69 ± 15	34 ± 15	10 ± 4	25 ± 2*

For detailed statistics see Suppl. Table 7.

DOI, 2,5-Dimethoxy-4-iodoamphetamine; PCP, phencyclidine; PTZ, Pentylenetetrazol

Acknowledgments

This work was supported by Inserm, Fondation pour la Recherche Médicale (FRM) and The French National Research Agency ANR-DOPAFEAR (EV), ANR-SEXREV (FV). GG is supported by Allen Foundation Inc. (2016.326) and Nutricia Research Foundation (2017-20) grants. The authors thank the animal breeding facility of Montpellier University (CECEMA).

References

Allen M. D., Zhang J. (2006) Subcellular dynamics of protein kinase A activity visualized by FRET-based reporters. *Biochem. Biophys. Res. Commun.* **348**, 716–721.

Balleine B. W., Delgado M. R., Hikosaka O. (2007) The role of the dorsal striatum in reward and decision-making. *J. Neurosci.* **27**, 8161–8165.

Beaulieu J.-M., Gainetdinov R. R. (2011) The physiology, signaling, and pharmacology of dopamine receptors. *Pharmacol. Rev.* **63**, 182–217.

Belin D., Jonkman S., Dickinson A., Robbins T. W., Everitt B. J. (2009) Parallel and interactive learning processes within the basal ganglia: relevance for the understanding of addiction. *Behav. Brain Res.* **199**, 89–102.

Berkeley J. L., Decker M. J., Levey A. I. (2002) The role of muscarinic acetylcholine receptor-mediated activation of extracellular signal-regulated kinase 1/2 in pilocarpine-induced seizures. *J. Neurochem.* **82**, 192–201.

Bertran-Gonzalez J., Bosch C., Maroteaux M., Matamales M., Hervé D., Valjent E., Girault J.-A. (2008) Opposing patterns of signaling activation in dopamine D1 and D2 receptor-expressing striatal neurons in response to cocaine and haloperidol. *J. Neurosci.* **28**, 5671–5685.

Bertran-Gonzalez J., Hervé D., Girault J.-A., Valjent E. (2010) What is the Degree of Segregation between Striatonigral and Striatopallidal Projections? *Front Neuroanat* **4**.

Biever A., Puighermanal E., Nishi A., David A., Panciatici C., Longueville S., Xirodimas D., et al. (2015) PKA-dependent phosphorylation of ribosomal protein S6 does not correlate with translation efficiency in striatonigral and striatopallidal medium-sized spiny neurons. *J. Neurosci.* **35**, 4113–4130.

Castro L. R. V., Brito M., Guiot E., Polito M., Korn C. W., Hervé D., Girault J.-A., Paupardin-Tritsch D., Vincent P. (2013) Striatal neurones have a specific ability to respond to phasic dopamine release. *J. Physiol. (Lond.)* **591**, 3197–3214.

Chevret P., Dobigny G. (2005) Systematics and evolution of the subfamily Gerbillinae (Mammalia, Rodentia, Muridae). *Mol. Phylogenet. Evol.* **35**, 674–688.

Choe E. S., Chung K. T., Mao L., Wang J. Q. (2002) Amphetamine increases phosphorylation of extracellular signal-regulated kinase and transcription factors in the rat striatum via group I metabotropic glutamate receptors. *Neuropsychopharmacology* **27**, 565–575.

Davis M. I., Puhl H. L. (2011) Nr4a1-eGFP is a marker of striosome-matrix architecture, development and activity in the extended striatum. *PLoS ONE* **6**, e16619.

Deniau J. M., Menetrey A., Charpier S. (1996) The lamellar organization of the rat substantia nigra pars reticulata: segregated patterns of striatal afferents and relationship to the topography of corticostriatal projections. *Neuroscience* **73**, 761–781.

Fasano S., D'Antoni A., Orban P. C., Valjent E., Putignano E., Vara H., Pizzorusso T., et al. (2009) Ras-guanine nucleotide-releasing factor 1 (Ras-GRF1) controls activation of extracellular signal-regulated kinase (ERK) signaling in the striatum and long-term behavioral responses to cocaine. *Biol. Psychiatry* **66**, 758–768.

Franklin, K. and Paxinos, G. K. (2008) *The Mouse Brain in Stereotaxic Coordinates, 3rd Edn*. Elsevier.

Fudge J. L., Haber S. N. (2002) Defining the caudal ventral striatum in primates: cellular and histochemical features. *J. Neurosci.* **22**, 10078–10082.

Gagnon D., Petryszyn S., Sanchez M. G., Bories C., Beaulieu J. M., De Koninck Y., Parent A., Parent M. (2017) Striatal Neurons Expressing D1 and D2 Receptors are Morphologically Distinct and Differently Affected by Dopamine Denervation in Mice. *Sci Rep* **7**, 41432.

Gangarossa G., Di Benedetto M., O'Sullivan G. J., Dunleavy M., Alcacer C., Bonito-Oliva A., Henshall D. C., Waddington J. L., Valjent E., Fisone G. (2011) Convulsant doses of a dopamine D1 receptor agonist result in Erk-dependent increases in Zif268 and Arc/Arg3.1 expression in mouse dentate gyrus. *PLoS ONE* **6**, e19415.

Gangarossa G., Espallergues J., Kerchove d'Exaerde A. de, El Mestikawy S., Gerfen C. R., Hervé D., Girault J.-A., Valjent E. (2013a) Distribution and compartmental organization of GABAergic medium-sized spiny neurons in the mouse nucleus accumbens. *Front Neural Circuits* **7**, 22.

Gangarossa G., Espallergues J., Mailly P., De Bundel D., Kerchove d'Exaerde A. de, Hervé D., Girault J.-A., Valjent E., Krieger P. (2013b) Spatial distribution of D1R- and D2R-expressing medium-sized spiny neurons differs along the rostro-caudal axis of the mouse dorsal striatum. *Front Neural Circuits* **7**, 124.

Gangarossa G., Perroy J., Valjent E. (2013c) Combinatorial topography and cell-type specific regulation of the ERK pathway by dopaminergic agonists in the mouse striatum. *Brain Struct Funct* **218**, 405–419.

Gangarossa G., Perroy J., Valjent E. (2013d) Combinatorial topography and cell-type specific regulation of the ERK pathway by dopaminergic agonists in the mouse striatum. *Brain Struct Funct* **218**, 405–419.

Gerfen C. R., Miyachi S., Paletzki R., Brown P. (2002) D1 dopamine receptor supersensitivity in the dopamine-depleted striatum results from a switch in the regulation of ERK1/2/MAP kinase. *J. Neurosci.* **22**, 5042–5054.

Gerfen C. R., Paletzki R., Worley P. (2008) Differences between dorsal and ventral striatum in Drd1a dopamine receptor coupling of dopamine- and cAMP-regulated phosphoprotein-32 to activation of extracellular signal-regulated kinase. *J. Neurosci.* **28**, 7113–7120.

Gerfen C. R., Surmeier D. J. (2011) Modulation of striatal projection systems by dopamine. *Annu. Rev. Neurosci.* **34**, 441–466.

Girault J.-A., Valjent E., Caboche J., Hervé D. (2007) ERK2: a logical AND gate critical for drug-induced plasticity? *Curr Opin Pharmacol* **7**, 77–85.

Gokce O., Stanley G. M., Treutlein B., Neff N. F., Camp J. G., Malenka R. C., Rothwell P. E., Fuccillo M. V., Südhof T. C., Quake S. R. (2016) Cellular Taxonomy of the Mouse Striatum as Revealed by Single-Cell RNA-Seq. *Cell Rep* **16**, 1126–1137.

Gong S., Zheng C., Doughty M. L., Losos K., Didkovsky N., Schambra U. B., Nowak N. J., et al. (2003) A gene expression atlas of the central nervous system based on bacterial artificial chromosomes. *Nature* **425**, 917–925.

Graybiel A. M., Grafton S. T. (2015) The striatum: where skills and habits meet. *Cold Spring Harb Perspect Biol* **7**, a021691.

Gruber A. J., McDonald R. J. (2012) Context, emotion, and the strategic pursuit of goals: interactions among multiple brain systems controlling motivated behavior. *Front Behav Neurosci* **6**, 50.

Guo L., Walker W. I., Ponvert N. D., Penix P. L., Jaramillo S. (2018) Stable representation of sounds in the posterior striatum during flexible auditory decisions. *Nat Commun* **9**, 1534.

Hintiryan H., Foster N. N., Bowman I., Bay M., Song M. Y., Gou L., Yamashita S., et al. (2016) The mouse cortico-striatal projectome. *Nat. Neurosci.* **19**, 1100–1114.

Huerta-Ocampo I., Mena-Segovia J., Bolam J. P. (2014) Convergence of cortical and thalamic input to direct and indirect pathway medium spiny neurons in the striatum. *Brain Struct Funct* **219**, 1787–1800.

Hunnicutt B. J., Jongbloets B. C., Birdsong W. T., Gertz K. J., Zhong H., Mao T. (2016) A comprehensive excitatory input map of the striatum reveals novel functional organization. *Elife* **5**.

Hutton S. R., Otis J. M., Kim E. M., Lamsal Y., Stuber G. D., Snider W. D. (2017) ERK/MAPK Signaling Is Required for Pathway-Specific Striatal Motor Functions. *J. Neurosci.* **37**, 8102–8115.

Jiang H., Kim H. F. (2018) Anatomical Inputs From the Sensory and Value Structures to the Tail of the Rat Striatum. *Front Neuroanat* **12**, 30.

Jiang S. Z., Xu W., Emery A. C., Gerfen C. R., Eiden M. V., Eiden L. E. (2017) NCS-Rapgef2, the Protein Product of the Neuronal Rapgef2 Gene, Is a Specific Activator of D1 Dopamine Receptor-Dependent ERK Phosphorylation in Mouse Brain. *eNeuro* **4**.

Jin D.-Z., Mao L.-M., Wang J. Q. (2019) Amphetamine activates non-receptor tyrosine kinase Fyn and stimulates ERK phosphorylation in the rat striatum in vivo. *Eur. J. Pharmacol.* **843**, 45–54.

Jin L.-Q., Goswami S., Cai G., Zhen X., Friedman E. (2003) SKF83959 selectively regulates phosphatidylinositol-linked D1 dopamine receptors in rat brain. *J. Neurochem.* **85**, 378–386.

Jolkkonen E., Pikkarainen M., Kemppainen S., Pitkänen A. (2001) Interconnectivity between the amygdaloid complex and the amygdalostriatal transition area: a PHA-L study in rat. *J. Comp. Neurol.* **431**, 39–58.

Kuroiwa M., Bateup H. S., Shuto T., Higashi H., Tanaka M., Nishi A. (2008) Regulation of DARPP-32 phosphorylation by three distinct dopamine D1-like receptor signaling pathways in the neostriatum. *J. Neurochem.* **107**, 1014–1026.

Lee S.-M., Kant A., Blake D., Murthy V., Boyd K., Wyrick S. J., Mailman R. B. (2014) SKF-83959 is not a highly-biased functionally selective D1 dopamine receptor ligand with activity at phospholipase C. *Neuropharmacology* **86**, 145–154.

Litjens R. P. W., Brunt T. M., Alderliefste G.-J., Westerink R. H. S. (2014) Hallucinogen persisting perception disorder and the serotonergic system: a comprehensive review including new MDMA-related clinical cases. *Eur Neuropsychopharmacol* **24**, 1309–1323.

Liu F. C., Graybiel A. M. (1998) Region-dependent dynamics of cAMP response element-binding protein phosphorylation in the basal ganglia. *Proc. Natl. Acad. Sci. U.S.A.* **95**, 4708–4713.

Matamales M., Bertran-Gonzalez J., Salomon L., Degos B., Deniau J.-M., Valjent E., Hervé D., Girault J.-A. (2009) Striatal medium-sized spiny neurons: identification by nuclear staining and study of neuronal subpopulations in BAC transgenic mice. *PLoS ONE* **4**, e4770.

Menegas W., Akiti K., Amo R., Uchida N., Watabe-Uchida M. (2018) Dopamine neurons projecting to the posterior striatum reinforce avoidance of threatening stimuli. *Nat. Neurosci.* **21**, 1421–1430.

Menegas W., Babayan B. M., Uchida N., Watabe-Uchida M. (2017) Opposite initialization to novel cues in dopamine signaling in ventral and posterior striatum in mice. *Elife* **6**.

Menegas W., Bergan J. F., Ogawa S. K., Isogai Y., Umadevi Venkataraju K., Osten P., Uchida N., Watabe-Uchida M. (2015) Dopamine neurons projecting to the posterior striatum form an anatomically distinct subclass. *Elife* **4**, e10032.

Nagai T., Yoshimoto J., Kannon T., Kuroda K., Kaibuchi K. (2016) Phosphorylation Signals in Striatal Medium Spiny Neurons. *Trends Pharmacol. Sci.* **37**, 858–871.

Nicola S. M. (2007) The nucleus accumbens as part of a basal ganglia action selection circuit. *Psychopharmacology (Berl.)* **191**, 521–550.

Nishi A., Kuroiwa M., Miller D. B., O'Callaghan J. P., Bateup H. S., Shuto T., Sotogaku N., et al. (2008) Distinct roles of PDE4 and PDE10A in the regulation of cAMP/PKA signaling in the striatum. *J. Neurosci.* **28**, 10460–10471.

Pascoli V., Besnard A., Hervé D., Pagès C., Heck N., Girault J.-A., Caboche J., Vanhoutte P. (2011) Cyclic adenosine monophosphate-independent tyrosine phosphorylation of NR2B mediates cocaine-induced extracellular signal-regulated kinase activation. *Biol. Psychiatry* **69**, 218–227.

Polito M., Guiot E., Gangarossa G., Longueville S., Doulazmi M., Valjent E., Hervé D., et al. (2015) Selective Effects of PDE10A Inhibitors on Striatopallidal Neurons Require Phosphatase Inhibition by DARPP-32. *eNeuro* **2**.

Polito M., Vincent P., Guiot E. (2014) Biosensor imaging in brain slice preparations. *Methods Mol. Biol.* **1071**, 175–194.

Poulin J.-F., Caronia G., Hofer C., Cui Q., Helm B., Ramakrishnan C., Chan C. S., Dombeck D. A., Deisseroth K., Awatramani R. (2018) Mapping projections of molecularly defined dopamine neuron subtypes using intersectional genetic approaches. *Nat. Neurosci.* **21**, 1260–1271.

Poulin J.-F., Zou J., Drouin-Ouellet J., Kim K.-Y. A., Cicchetti F., Awatramani R. B. (2014) Defining midbrain dopaminergic neuron diversity by single-cell gene expression profiling. *Cell Rep* **9**, 930–943.

Ren K., Guo B., Dai C., Yao H., Sun T., Liu X., Bai Z., Wang W., Wu S. (2017) Striatal Distribution and Cytoarchitecture of Dopamine Receptor Subtype 1 and 2: Evidence from Double-Labeling Transgenic Mice. *Front Neural Circuits* **11**, 57.

Root D. H., Wang H.-L., Liu B., Barker D. J., Mód L., Szocsics P., Silva A. C., Maglóczky Z., Morales M. (2016) Glutamate neurons are intermixed with midbrain dopamine neurons in nonhuman primates and humans. *Sci Rep* **6**, 30615.

Saunders A., Macosko E. Z., Wysoker A., Goldman M., Krienen F. M., Rivera H. de, Bien E., et al. (2018) Molecular Diversity and Specializations among the Cells of the Adult Mouse Brain. *Cell* **174**, 1015-1030.e16.

Starr M. A., Page M. E., Waterhouse B. D. (2008) MDMA (3,4-methylenedioxymethamphetamine)-mediated distortion of somatosensory signal transmission and neurotransmitter efflux in the ventral posterior medial thalamus. *J. Pharmacol. Exp. Ther.* **327**, 20–31.

Valjent E., Pascoli V., Svenningsson P., Paul S., Enslen H., Corvol J.-C., Stipanovich A., et al. (2005) Regulation of a protein phosphatase cascade allows convergent dopamine and glutamate signals to activate ERK in the striatum. *Proc. Natl. Acad. Sci. U.S.A.* **102**, 491–496.

Veyrunes F., Dobigny G., Yang F., O'Brien P. C. M., Catalan J., Robinson T. J., Britton-Davidian J. (2006) Phylogenomics of the genus Mus (Rodentia; Muridae): extensive genome repatterning is not restricted to the house mouse. *Proc. Biol. Sci.* **273**, 2925–2934.

Wei X., Ma T., Cheng Y., Huang C. C. Y., Wang X., Lu J., Wang J. (2018) Dopamine D1 or D2 receptor-expressing neurons in the central nervous system. *Addict Biol* **23**, 569–584.

Xiong Q., Znamenskiy P., Zador A. M. (2015) Selective corticostriatal plasticity during acquisition of an auditory discrimination task. *Nature* **521**, 348–351.

Yamamoto T., Ueji K. (2011) Brain mechanisms of flavor learning. *Front Syst Neurosci* **5**, 76.

Yapo C., Nair A. G., Clement L., Castro L. R., Hellgren Kotaleski J., Vincent P. (2017) Detection of phasic dopamine by D1 and D2 striatal medium spiny neurons. *J. Physiol. (Lond.)* **595**, 7451–7475.

Yin H. H., Knowlton B. J. (2006) The role of the basal ganglia in habit formation. *Nat. Rev. Neurosci.* **7**, 464–476.

Figure Legends

Figure 1: Distribution of D1R- and D2R-SPNs in the tail of the striatum. (a) RFP (magenta) and GFP (cyan) immunofluorescence in the TS of *Drd2*-eGFP/*Drd1a*-dtTomato mice. Scale bar, 200 µm. Schematic cartoon illustrating the distribution of GFP-, RFP- and GFP/RFP-expressing neurons. (b) High magnification of the AST of *Drd2*-eGFP/*Drd1a*-dtTomato mice. Scale bar, 20 µm. Distribution expressed as a percentage of neurons expressing GFP (D2R), RFP (D1R) or both GFP/RFP (D2R/D1R). (c) Double immunofluorescence of D2R, A2aR (yellow), D1R (magenta) and GFP (Cyan) in the TS of *Drd2*-eGFP mice. Scale bar, 200 µm. Cx: Cortex; cc: corpus callosum; GPe: external globus pallidus; AST: amygdalostriatal transition; LA: lateral amygdala.

Figure 2: PKA imaging following activation of D1R and A2aR in the tail of the striatum. Wide-field imaging of mouse striatal brain slices expressing AKAR3 biosensor in D2R/A2aR-lacking (a, b) and in the AST (c, d) areas. (a, c) Raw fluorescence of the acceptor is displayed in gray and acceptor/donor fluorescence is displayed in pseudo-color, coded from blue (low F535/F480 ratio, ie low PKA signal) to red (high PKA signal). Ratio images (a-d) correspond to the time points indicated in the bottom graph. Changes in ratio were measured during time and each trace indicates the F535/F480 emission ratio measured on the region of interest of corresponding color shown on the gray image. Traces in gray correspond to regions of interest outside the selected region of the field. The thick black trace represents the average. Horizontal bars indicate the bath application of SKF38393 (1µM), CGS21680 (1µM) and forskolin (Fsk, 12.5 µM). (b, d) Amplitude of the F535/F480 emission ratio triggered by SKF38393 (SKF) and CGS21680 (CGS) in the

D2R/A2aR-lacking area (b, top graph) and the AST (d, bottom graph). Mean ± sem is represented by the filled circles. CGS21680 vs SKF38393 *** $p < 0.001$.

Figure 3: The D2R/A2aR-lacking area is evolutionary conserved. (a) Simplified phylogenetic tree and divergence time estimates of the *Mus* species group, according to (Chevret and Dobigny 2005; Veyrunes *et al.* 2006). Species identified in magenta have been used in the present study. (b-e) Double immunofluorescence of A2aR (magenta) and DARPP-32 (yellow) in the TS of (b) 3 subspecies of the *Mus musculus* [*Mus m. domesticus* (DCA), the *Mus m. castaneus* (CIM) and the *Mus musculus* (KAK), c) 4 species of *Subgenus Mus* [*Mus spretus* (SMZ), *Mus spicilegus* (ZRU), *Mus macedonicus* (XBS) and *Mus caroli* (KTK)] and 2 species from other *Subgenera* (*Nannomys minutoides* and *Coelomys pahari*). Scale bar, 250 µm, (d) in *Meriones unguiculatus* (Mongolian gerbil). Scale bar, 200 µm, and (e) in *Rattus norvegicus.* Scale bar, 250 µm. White arrowheads delineate the boundaries between the intermingled area and D2R/A2aR-lacking area. Cx: Cortex; GPe: external globus pallidus; TS: tail of the striatum.

Figure 4: Regulation of ERK phosphorylation in the TS by d-amphetamine. (a) P-ERK immunoreactivity (magenta) in the TS of C57/Bl6 mice 15 min after saline or d-amphetamine (10 mg/kg) administration. Scale bar, 100 µm. (b) Quantification of P-ERK-immunoreactive neurons in the intermingled area, the D2R/A2aR-lacking area and the AST of mice treated with saline or d-amphetamine and perfused 15 or 30 min after injection. Data are presented as box and whisker plots. (c) P-ERK (magenta) and GFP (cyan) immunoreactivity in the TS of *Drd2*-eGFP mice 15 min after saline or d-amphetamine (10 mg/kg) administration. Scale bar, 100 µm. (d) Quantification of P-

ERK-immunoreactive neurons among eGFP-positive (D2R+) or eGFP-negative (D2R-) cells in the intermingled area, the D2R/A2aR-lacking area and the AST of *Drd2*-eGFP mice treated saline or d-amphetamine and perfused 15 or 30 min after injection. Data are presented as means ± sem. (e) P-ERK (magenta) and GFP (cyan) immunoreactivity in the TS of *Nr4a1*-eGFP mice 15 min after saline or d-amphetamine (10 mg/kg) administration. Scale bar, 100 µm. (f) Same quantifications as in (d) performed in *Nr4a1*-eGFP mice. Data are presented as means ± sem. * $p < 0.05$, ** $p < 0.01$, *** $p < 0.001$ sal vs d-amph. For detailed statistics see Suppl. Table 1. GPe: external globus pallidus; AST: amygdalostriatal transition; LA: lateral amygdala; sal: saline; d-amph: d-amphetamine.

Figure 5: Psychostimulants increase ERK phosphorylation in the TS. (a) P-ERK (magenta) and GFP (cyan) immunoreactivity in the TS of *Drd2*-eGFP mice 15 min after saline, methylphenidate (15 mg/kg), MDMA (10 mg/kg) or cocaine (15 mg/kg) administration. Scale bar, 200 µm. (b) Quantification of P-ERK-immunoreactive neurons in the intermingled area, the D2R/A2aR-lacking area and the AST of mice treated with saline, methylphenidate (15 mg/kg), MDMA (10 mg/kg) or cocaine (15 mg/kg). Data are presented as box and whisker plots. (c) Quantification of P-ERK-immunoreactive neurons among eGFP-positive (D2R+) or eGFP-negative (D2R-) cells in the intermingled area, the D2R/A2aR-lacking area and the AST of *Drd2*-eGFP mice treated saline, methylphenidate (15 mg/kg), MDMA (10 mg/kg) or cocaine (15 mg/kg) administration or d-amphetamine and perfused 15 after injection. Data are presented as means ± sem. * $p < 0.05$, ** $p < 0.01$, *** $p < 0.001$ sal vs drugs. For detailed statistics see Suppl. Table 2. GPe: external globus pallidus; AST:

amygdalostriatal transition; LA: lateral amygdala; sal: saline; d-amph: d-amphetamine.

Figure 6: Dopamine reuptake inhibitor enhances ERK activation in the TS. (a) P-ERK (magenta) immunoreactivity in the TS of *C57/Bl6* mice 15 min after saline, GBR12783 (10 mg/kg), desipramine (20 mg/kg) or fluoxetine (10 mg/kg) administration. Scale bar, 100 µm. (b) Quantification of P-ERK-immunoreactive neurons in the intermingled area, the D2R/A2aR-lacking area and the AST of mice treated with saline, GBR12783 (10 mg/kg), desipramine (20 mg/kg) or fluoxetine (10 mg/kg). Data are presented as box and whisker plots. * $p < 0.05$, *** $p < 0.001$ sal vs drugs. For detailed statistics see Suppl. Table 3. GPe: external globus pallidus; AST: amygdalostriatal transition; LA: lateral amygdala.

Figure 7: Distinct pattern of ERK phosphorylation in the TS by D1R agonists and PDE inhibitors. (a) P-ERK (magenta) immunofluorescence in the TS of d-amphetamine-injected mice, in the presence or not of a D1R antagonist (sch) injected 15 min before d-amphetamine. Scale bar, 200 µm. (b) Quantification of P-ERK-immunoreactive neurons in the intermingled area, the D2R/A2aR-lacking area and the AST of mice treated d-amphetamine alone or with SCH23390. Data are presented as box and whisker plots. * $p < 0.05$, ** $p < 0.01$ veh/d-amph vs sch/d-amph (c) P-ERK (magenta) immunofluorescence in the TS of mice injected with saline, various D1R agonists (SKF81297, SKF83822 and SKF83959 (5 mg/kg) or the non-selective D1R/D2R agonist, apomorphine (3 mg/kg). Scale bar, 200 µm. (d) P-ERK (magenta) and GFP (cyan) immunolabelling in the TS of *Drd2*-eGFP mice 15 min after saline or papaverine (30 mg/kg) administration. Scale bar, 200 µm. (e)

Quantification of P-ERK-immunoreactive neurons in the intermingled area, the D2R/A2aR-lacking area and the AST of mice treated with saline saline or papaverine (30 mg/kg). Data are presented as box and whisker plots. (f) Quantification of P-ERK-immunoreactive neurons among eGFP-positive (D2R+) or eGFP-negative (D2R-) cells in the intermingled area, the D2R/A2aR-lacking area and the AST of *Drd2*-eGFP mice treated with saline or papaverine (30 mg/kg). Data are presented as means ± sem. (g and h) Same analysis and quantification as in (d) and (f) except that mice were treated with rolipram (10 mg/kg). * $p < 0.05$, ** $p < 0.01$, *** $p < 0.001$ sal vs drugs. For detailed statistics see Suppl. Table 4. GPe: external globus pallidus; AST: amygdalostriatal transition; LA: lateral amygdala; sch: SCH23390; veh: vehicle; sal: saline; d-amph: d-amphetamine.

Gangarossa et al., Figure 1

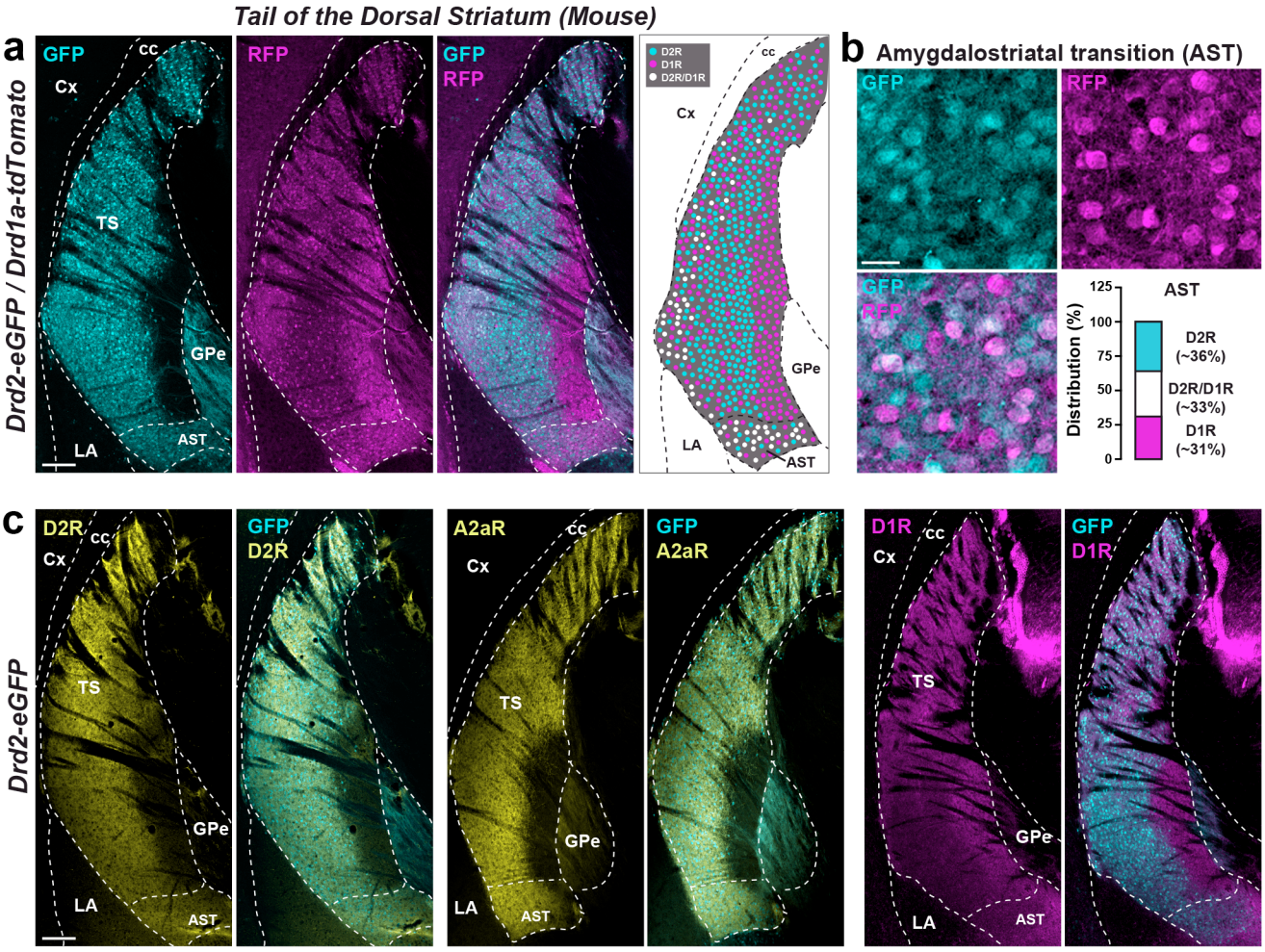

Gangarossa et al., Figure 2

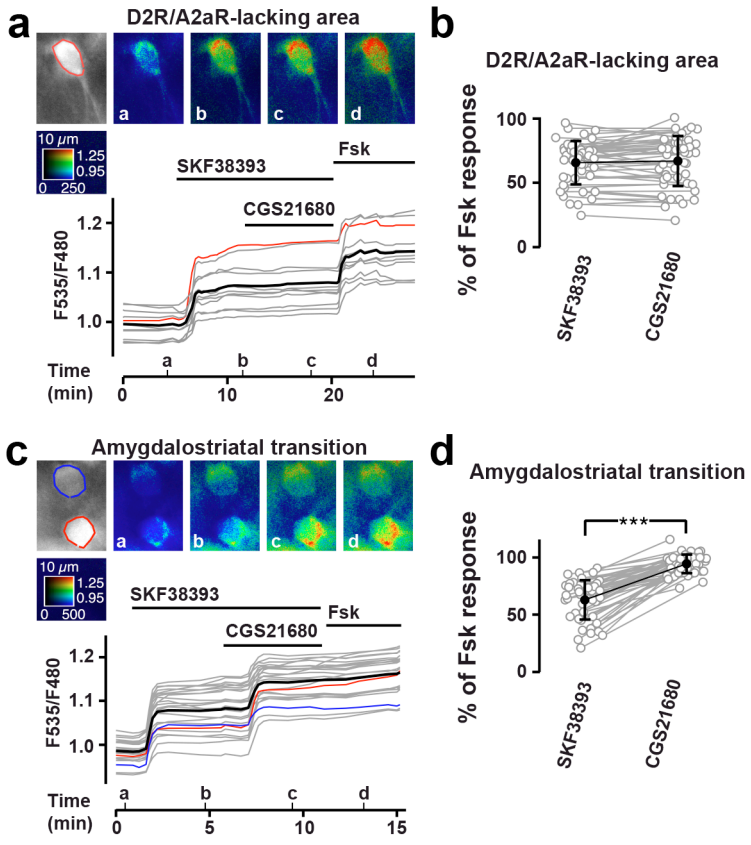

Gangarossa et al., Figure 3

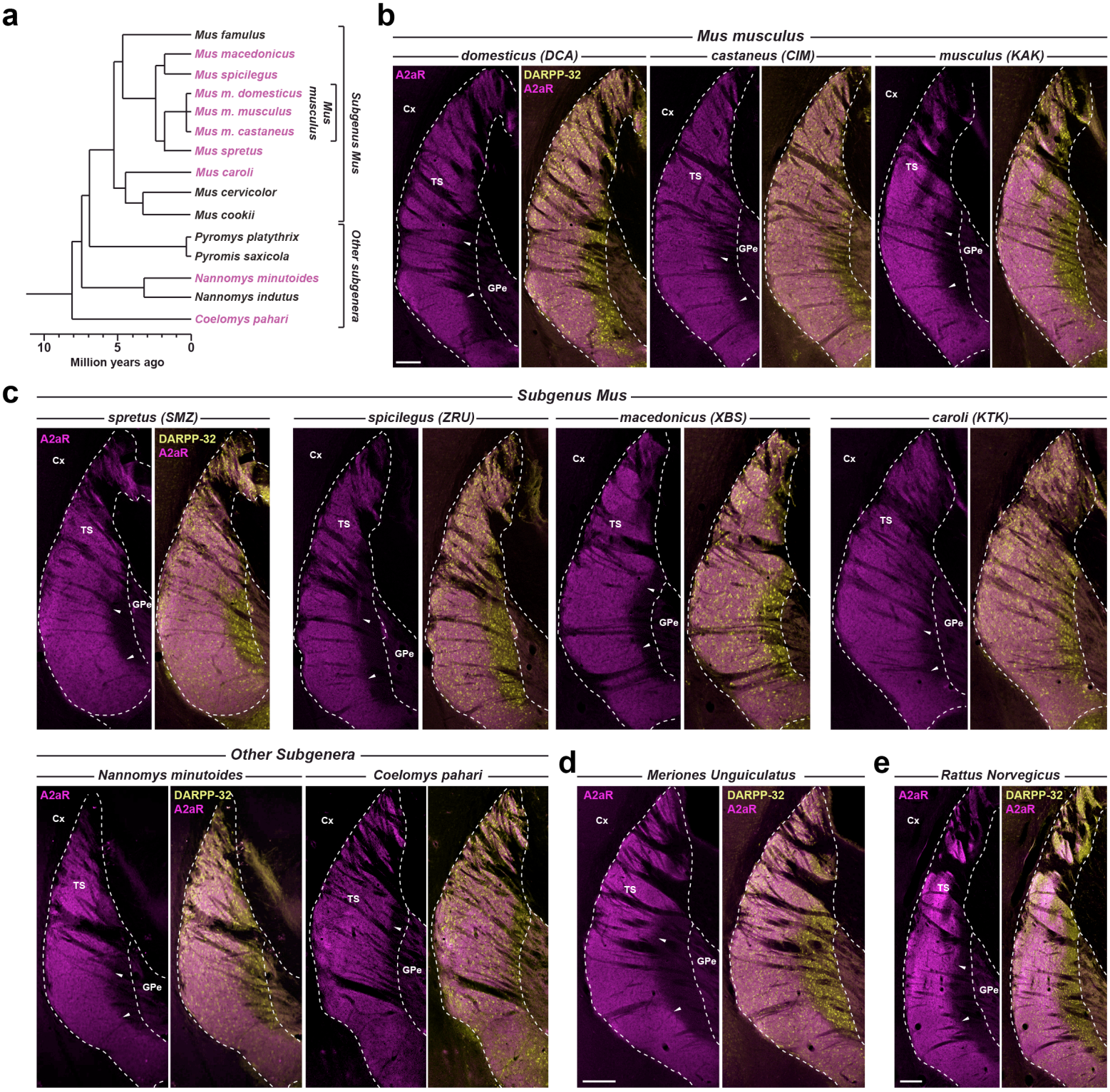

Gangarossa et al., Figure 4

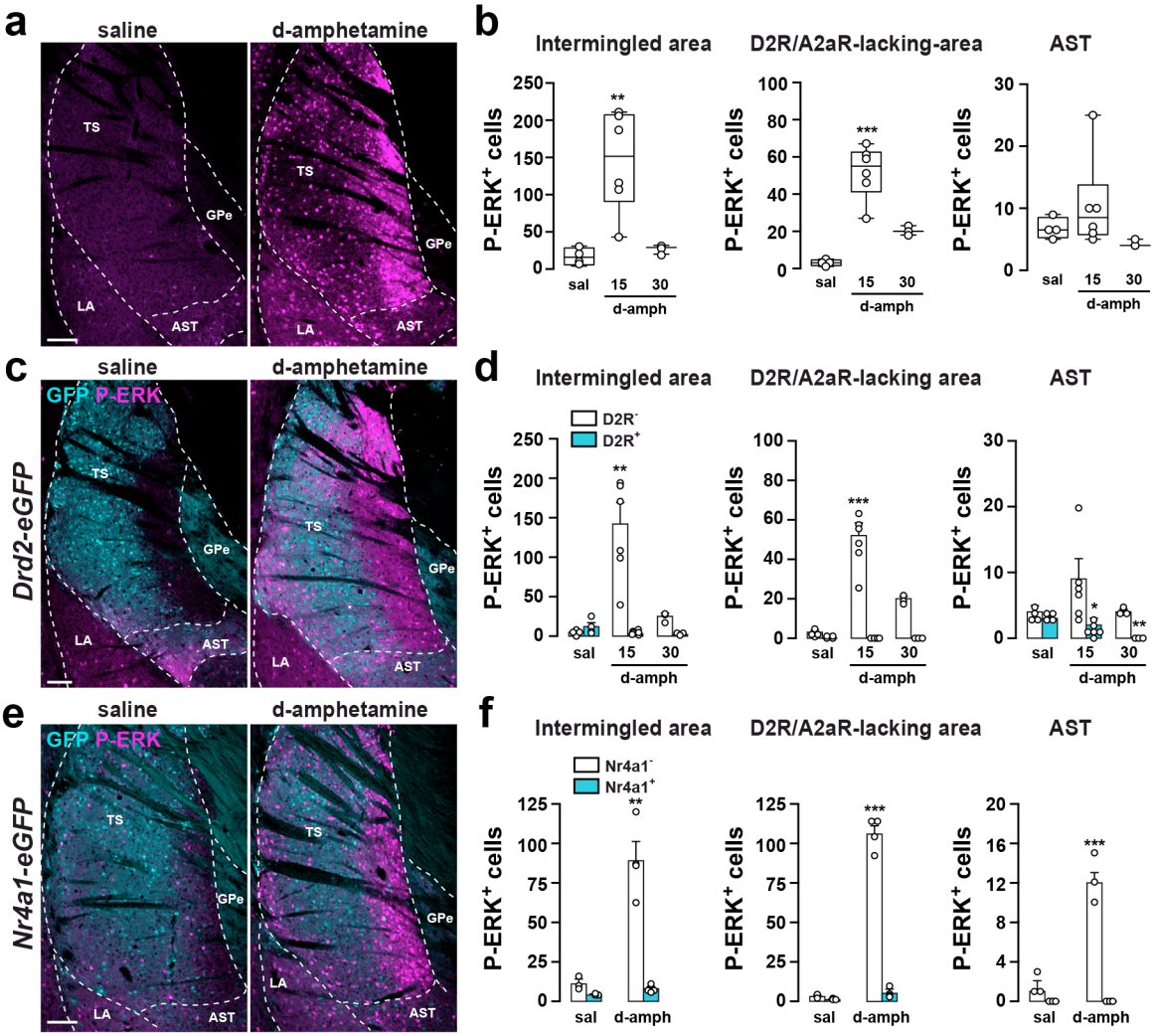

Gangarossa et al., Figure 5

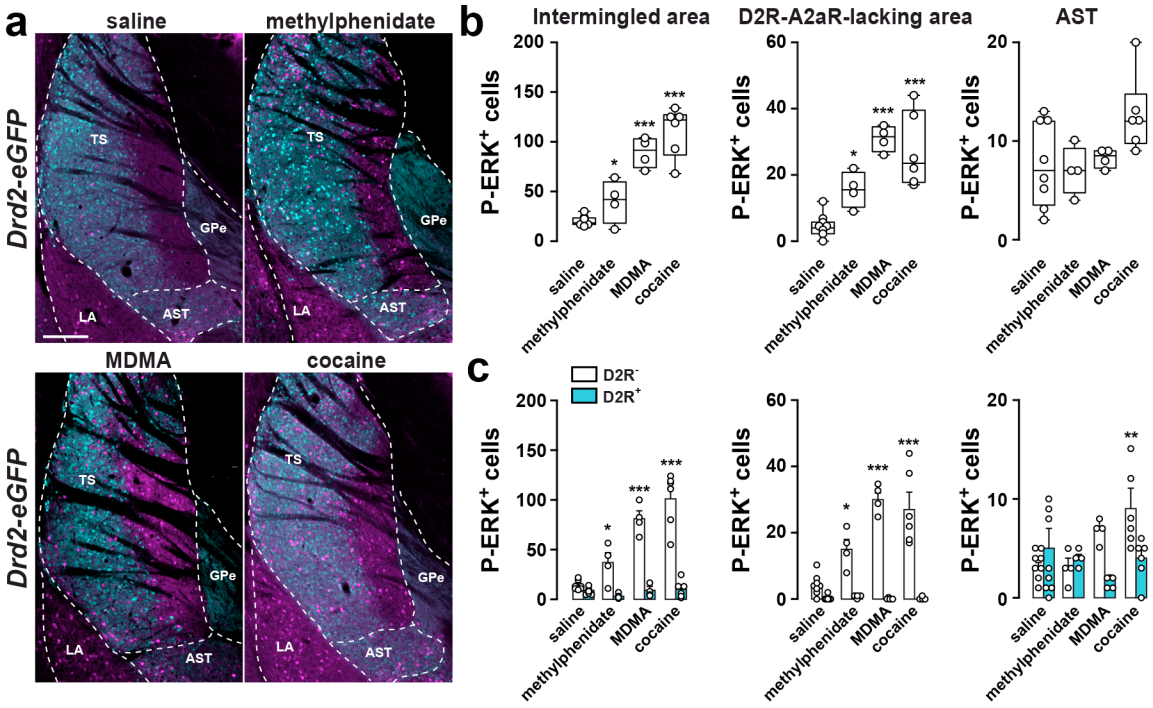

Gangarossa et al., Figure 6

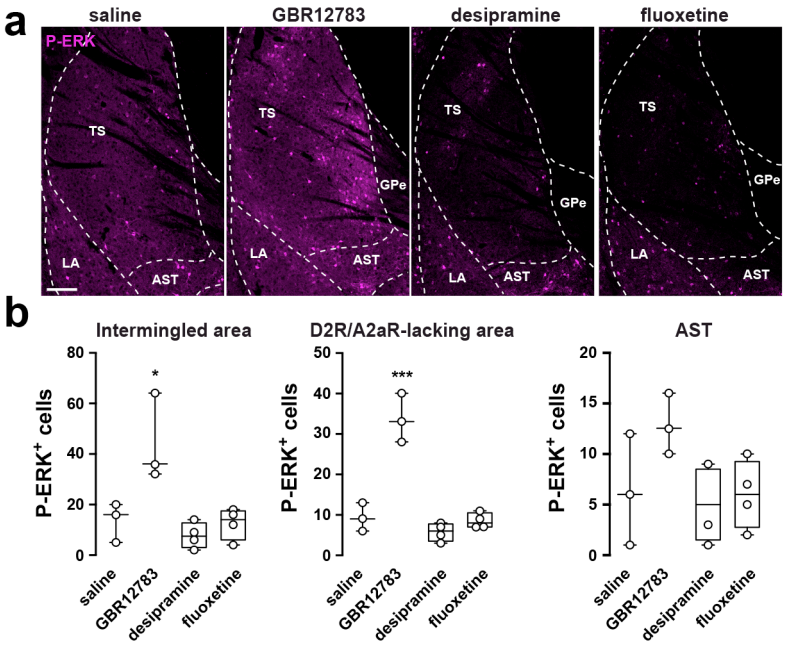
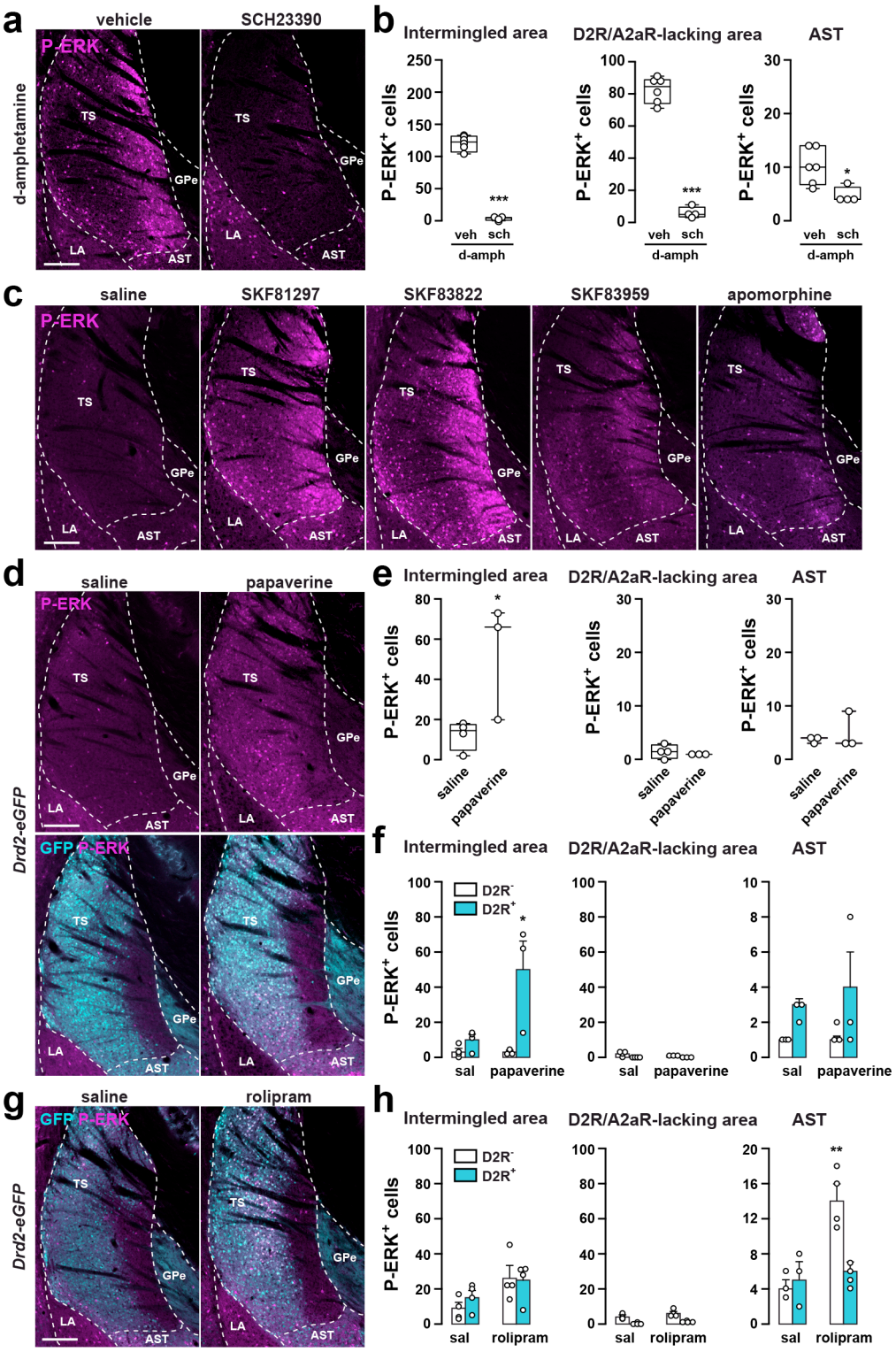
Gangarossa et al., Figure 7